Classical and Quantum Gravity

PAPER • **OPEN ACCESS**

Improved fused silica fibres for the advanced LIGO monolithic suspensions

To cite this article: Kyung-Ha Lee *et al* 2019 *Class. Quantum Grav.* **36** 185018

OPEN ACCESS
IOP Publishing
Classical and Quantum Gravity
Class. Quantum Grav. **36** (2019) 185018 (15pp)
https://doi.org/10.1088/1361-6382/ab28bd

Improved fused silica fibres for the advanced LIGO monolithic suspensions

Kyung-Ha Lee[1], Giles Hammond, James Hough, Russell Jones, Sheila Rowan and Alan Cumming

Kelvin Building, University of Glasgow, Glasgow G12 8QQ, United Kingdom

E-mail: k.lee.1@research.gla.ac.uk

Received 24 September 2018, revised 5 May 2019
Accepted for publication 11 June 2019
Published 28 August 2019

Abstract

To further increase the sensitivity of the advanced LIGO (aLIGO) gravitational wave detectors, two major upgrades of the monolithic fused silica suspension are considered: a higher stress in the suspension fibres and a longer final suspension stage. One of the challenges for this upgrade will be producing thinner and longer fibres that can hold the test mass safely. We demonstrate that laser power fluctuations during the fibre fabrication process can produce diameter variations and potentially weak fibres. We present a laser intensity stabilisation technology for fused silica fibre fabrication using a camera system to monitor heating. Fibres fabricated with this new technique showed a 34% decrease in the interquartile range of measured breaking stress, which indicates that the application of intensity stabilisation technology can improve the statistical strength of fused silica fibres by tightening the spread of values. As the aLIGO detectors upgrade plan (A+) proposes to use thinner fibres, it is essential to enhance the performance of fused silica fibres.

Keywords: gravitational wave, advanced LIGO, suspensions, fused silica, stabilisation

(Some figures may appear in colour only in the online journal)

1. Introduction

2015 was a defining year in both physics and astronomy, as a new means of observing the universe was unlocked with the detection of gravitational waves from a binary black hole

[1] Author to whom any correspondence should be addressed.

merger, GW150914, by the Advanced LIGO (aLIGO) ground based interferometric detector network [1]. Since that first detection, there have been 11 detections so far including binary black hole mergers (e.g. GW170814, GW170818) which were made along with the Advanced Virgo (AdVirgo), and GW170817, the first binary neutron star inspiral, also detected by both aLIGO and AdVirgo [2]. By having a network of detectors, independent verification of detections and sky localisation of gravitational wave sources was possible using triangulation [3].

Both aLIGO and AdVirgo utilise multi-stage pendulums with fused silica final stage to reduce the impact from thermal noise [4, 5]. In aLIGO, the installation of a quadruple pendulum system with a monolithic fused silica final stage made a significant contribution to improving the detector's sensitivity at lower frequencies [6–9]. Among various possible materials, fused silica has strong advantages such as low mechanical loss, convenience to fabricate and weld fibres to build a monolithic stage, and cancellation of thermoelastic noise by controlling the diameter of the fibres [10–13]. In this paper, an investigation into improved silica suspension fibre fabrication techniques will be the focus.

The main benefit that an upgraded monolithic final stage can bring is to further enhance sensitivity. Figure 1 shows the suspension thermal noise and other fundamental noise sources in aLIGO. Two resonances that can encroach into the detection band range are the vertical bounce mode (9.8 Hz) and the first violin mode (512 Hz). By lowering the vertical bounce mode frequency and pushing up the first violin mode frequency, the detection band will be expanded [15, 16]. It would be possible to achieve this with more highly stressed suspension fibres.

Additionally, the mass of the final stage mirror, and the length of the suspension fibres are possible upgrade parameters. Increasing the mass, as well as the fibre length can improve the base level of suspension thermal noise allowing enhanced detector sensitivity below 10 Hz and up to 20 Hz [17], and thus the observation time of astronomical events can be increased [18]. In addition, earlier warning and more accurate sky localisation would be possible, enhancing the chance to perform multi-messenger observations [19].

To achieve all of these proposed changes, it is crucial to be able to fabricate suspension fibres that are thin, long, and robust enough. Therefore, an in-depth investigation on developing fibre fabrication technology was performed to produce enhanced fused silica fibres suitable for future aLIGO upgraded suspensions. Implementation of a monitoring system for the intensity of heated silica stock and feedback system for the fibre pulling machine, along with various pulling and polishing conditions were studied. Strength tests and breaking point investigations were performed on the resulting fibres to confirm the impact of new fabrication technologies on their statistical strength and dimensional reproducibility. Finally, we will consider some credible suspension upgrade options that employ these fibres, and show their improved noise performance.

2. Enhanced fibre fabrication technologies

2.1. Current fibre fabrication technique

Fused silica fibres currently used for suspending the final mirror stage in aLIGO were produced using a bespoke pulling machine (figure 3(a)) [20]. The typical dimension of the current aLIGO fibre is 600 mm in length, 800 μm diameter in the thermoelastic null sections [21], 400 μm diameter in the thin middle section (figure 2).

A Synrad 120 W CO_2 laser (pulse width modulation rate of 10 kHz) is used to heat circular cross section fused silica stock material. A rotating 45° mirror (rotation speed of 62 Hz) and two conical mirrors allow uniform heating 360° around the stock. Since the strength of fibres

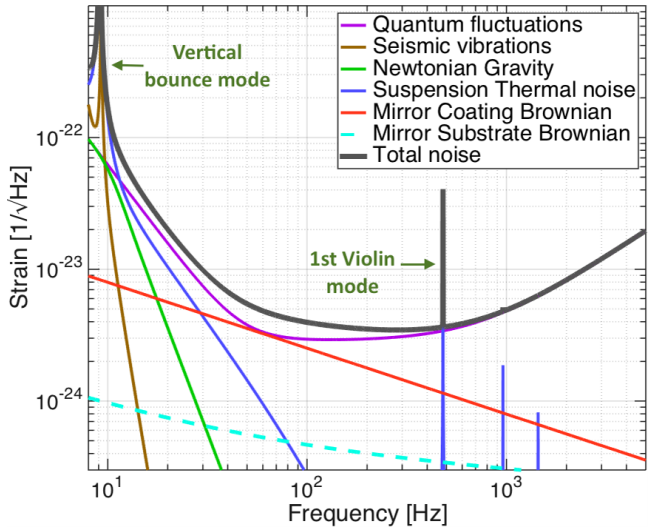

Figure 1. Modelled various noise sources in the aLIGO [14].

Figure 2. Dumbbell-shaped fibre for the aLIGO suspension system.

is directly related to the surface cracks of the silica stock [22], the stock is polished before the pull to improve the strength [23]. Polishing comprises of the lower stage moving up and down slowly (typically 0.1 mm s^{-1}) while the stock surface is uniformly heated to its melting point to smooth surface cracks.

The top clamp, which holds one end of the stock, is attached to the upper stage which can travel up and down, while the bottom clamp is attached to the base of the machine to keep it stationary. The conical mirror attached to the lower stage travels down to heat fresh material. To pull a fibre, the top clamp travels upwards while the bottom clamp is stationary. The geometry of the fibre is determined by the relative speeds of the upper and lower stages.

To date, the laser system has been run open loop where the duty cycle of the laser has been set manually. The laser power has been observed to vary throughout the polishing and the pulling process, particularly on startup. For first 400 s, the variations are more rapid and larger in amplitude, and as times goes by, they get smaller as Synrad's specification states. Although the power fluctuation is within the laser's specification which is $\pm 10\%$ for cold start and $\pm 6\%$ for 2 min thereafter, this instability becomes more critical when it is translated to the heating intensity of the silica stock. Variations in laser power have been observed to cause variation in the heating intensity of the molten fused silica stock material, which in turn may have an influence on the fibre geometry. To improve the intensity stability, a heating intensity monitoring and feedback system using a camera was set up and the impact of laser intensity stabilisation on the fibres was investigated.

2.2. Enhanced fibre fabrication technique with camera monitoring system and PID feedback control

There are four main challenges in monitoring the heating of silica stock. Firstly, the monitoring device cannot directly touch the stock, as the heating point of the stock is molten from the heat deposited by the laser beam. Any thermometer attached to the stock at its heating point will have direct exposure to the laser beam, because the stock is uniformly heated all round. In addition, the strength of silica fibres is very sensitive to the surface cracks and contaminations, and any direct contact on the surface of the stock can consequently lower the fibre strength. Secondly, since the pulling process happens quickly, the monitoring device must have fast response. Thirdly, the temperature monitoring device should be able to handle very high temperatures, around 2200 °C, which is the approximate melting point of fused silica. Finally, the temperature monitoring device should not be at a risk of damage due to reflected CO_2 laser light from the heating point. This condition eliminates infrared cameras, such as FLIR cameras [24], as their CCD sensors are very vulnerable to damage from exposure to CO_2 laser reflections. Since most thermometers are not qualified for all these conditions, a feedback system using a camera as an input was used to monitor the brightness of the heated stock from which we can monitor the heating intensity variation of the region. As fused silica glows as it gets heated, this camera system can act as a responsive optical pyrometer with brightness as a temperature proxy.

A Ximea MD028MU-SY camera was set up with suitable neutral-density filters to monitor the heating point of the fused silica stock without intensity saturation. To optimise the response time, the exposure was set to 8000 μs to maximise the frame rate (100 fps) while maintaining a reasonable resolution. Since the maximum pixel value was 16383 (14-bit), the setpoint chosen by eye was kept around the 5000–6000 range, with a neutral-density filter of 3.5 used to prevent saturation during the pull. Figure 3(c) shows an image of heated fused silica stock taken by the camera monitoring system.

A proportional integral derivative (PID) control system was implemented in the pulling machine's LabVIEW control program. The pixel data of a vertical line in the middle of the fibre was recorded, and the brightest pixel value was used to monitor the temperature. The heating power was stabilised by controlling its power via its dedicated analogue voltage input, to stabilise the brightest pixel value throughout the run.

Figure 4(a) shows the pixel intensity stability comparison between unstabilised and stabilised conditions while running the laser for 15 min while stationary on the silica stock. For the unstabilised run, the laser was run with a constant duty cycle of 39%. This run had significantly more fluctuations in brightness throughout, which indicates that the heating intensity of the stock was not kept constant due to laser power variations. As noted previously, fluctuations during first 400 s were more rapid and larger in amplitude, and they got smaller as time went on, which was the same behaviour observed and quoted by Synrad for this laser. When the stabilisation system was applied, the average peak pixel intensity was 5998 with an average standard deviation of 38.5, excluding the initial overshoot. Figure 4(b) shows standard deviation calculated over 100 points throughout the stabilised run, which conveys the level of stability achieved by the system.

Using this camera system, we were able to directly compare the correlation between heating intensity fluctuations and fibre geometry. For one of the pulls with continuous fluctuations in heating intensity, the corresponding fibre diameter was measured using a diameter profiler [25] and compared with the heating intensity data (figure 5). When there was a continuous sinusoidal fluctuation in the heating intensity, the diameter of the fibre also showed similar

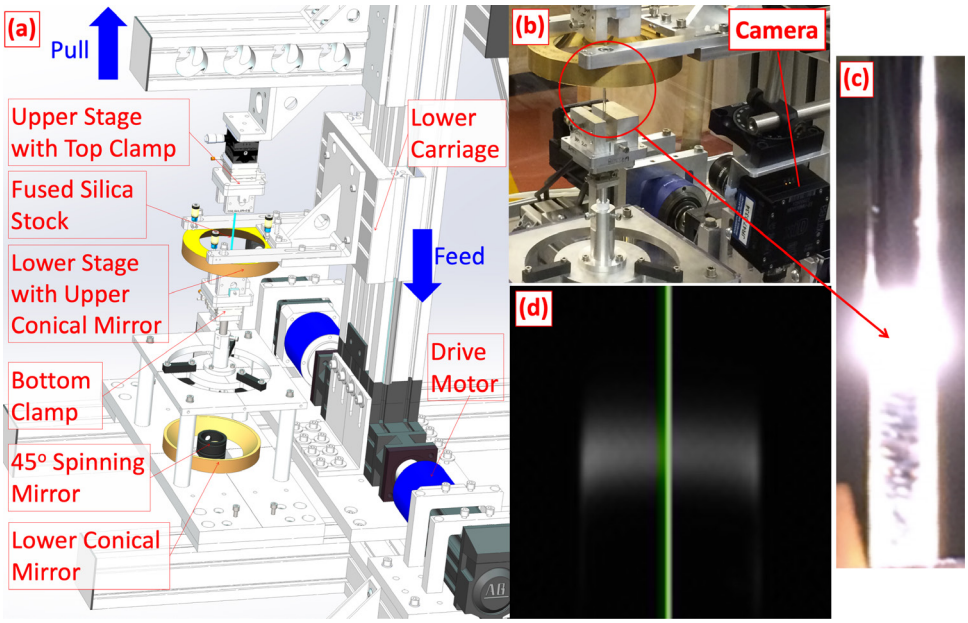

Figure 3. (a) Schematic drawing of the fused silica fibre pulling machine. (b) The fused silica fibre pulling machine with the camera feedback system. (c) Uniformly heated fused silica stock, as viewed by a camera (shown without neutral-density filters). (d) Image of the heating point taken by the camera. The green vertical line indicates the region where pixel data is taken.

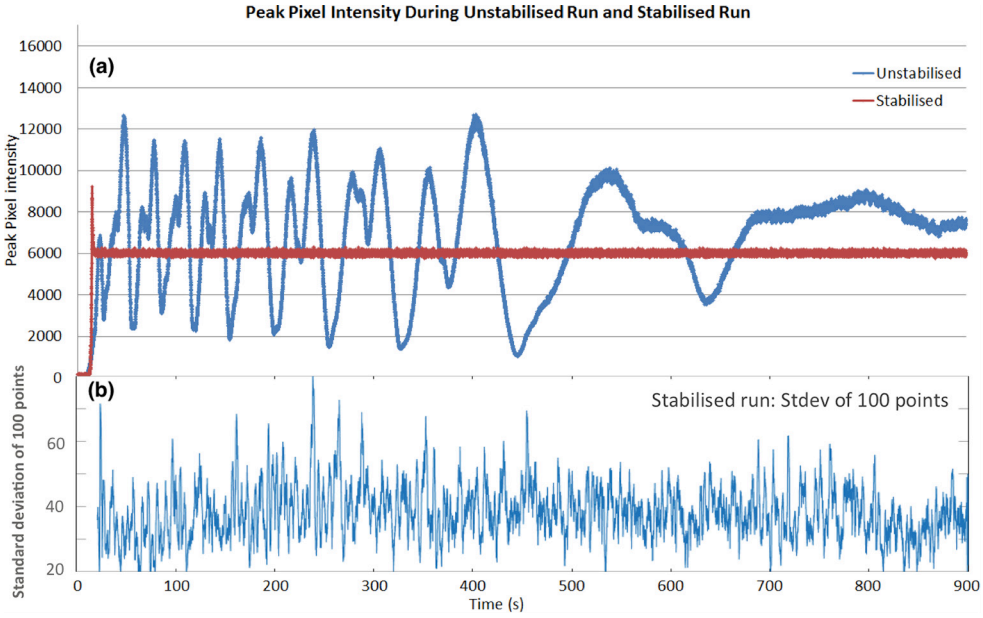

Figure 4. Peak pixel intensity comparison between unstabilised and stabilised conditions. Laser was on for 15 min for each run, while the pulling machine was kept stationary. The lower panel shows standard deviation over 100 points (duration of 2 s).

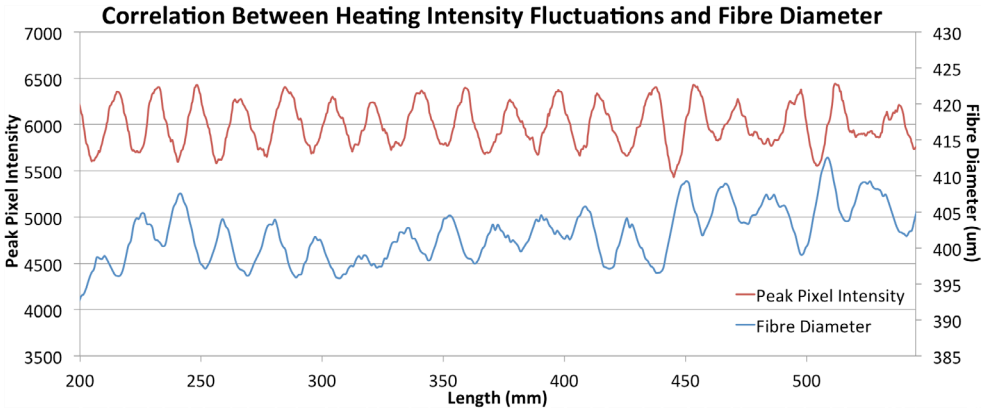

Figure 5. Correlation between heating intensity fluctuation and fibre geometry.

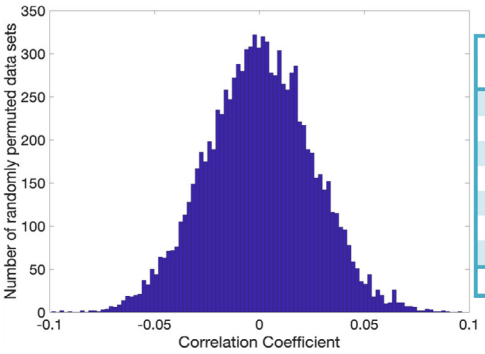

	Correlation Coefficient	Stdev of random distribution	Sigma
Fibre 1	0.2647	0.0256	10.34
Fibre 2	0.4614	0.0254	18.16
Fibre 3	0.2555	0.0258	9.903
Fibre 4	0.2151	0.0249	8.638
Fibre 5	0.1594	0.0254	6.275
Fibre 6	0.1521	0.0256	5.941
Fibre 7	0.3378	0.0257	13.14
AVERAGE	0.264	0.0255	10.34

Figure 6. (a) Histogram of correlation coefficients between peak pixel intensity and fibre diameter randomly permuted for 10 000 times. (b) Summary table presenting correlation coefficients of original datasets, FWHM and standard deviation of 10 000 randomly permuted datasets, and statistical significance sigma.

sinusoidal fluctuations. This behaviour was observed every time there were significant fluctuations in peak pixel intensity.

The correlation coefficient for the peak pixel intensity and diameter profile was determined using Matlab's *corrcoeff* function. To check the significance of this value, the data sets were randomly permuted 10 000 times and the correlation coefficient was recalculated for each case [26]. This calculation was repeated for seven different fibres. Figure 6(a) shows Fibre 1's result plotted in a histogram as an example. The correlation coefficients of a randomly permuted data set followed a gaussian distribution centred on zero with a standard deviation of 0.0256 (FWHM of 0.0494). Considering the correlation coefficient of the original data was 0.2647, it has 10.34 sigma away from the mean. The figure 6(b) shows the summary of the correlation analysis. The average statistical significance (sigma) from seven different fibres was 10.34, which gives a quantitative confirmation of a correlation between laser fluctuations and the resulting diameter of the fibres.

These data prove that there is a direct correlation between the heating intensity instability and the variation in the fibre diameter profile. These variations in the diameter can cause undesirable effects on fibres such as a tensile stress concentrations on the thinner areas. Therefore,

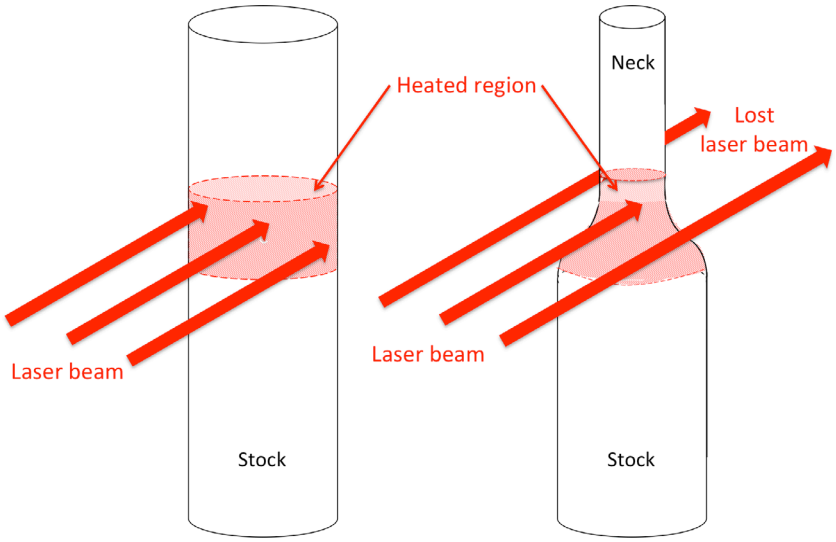

Figure 7. Loss of light due to a smaller fibre diameter.

by stabilising the heating intensity of the fused silica stock, there is a potential improvement in the dimensional reproducibility and statistical strength of the fibres.

2.3. Wait time and pull PID gain adjustment

As figure 4 shows, most of the critical laser fluctuations happened during the first 700 s after startup. With the stabilisation system, the time required to avoid those fluctuations decreased to 200 s. A few cases were observed where a big fluctuation happened after 200 s, so a buffer time of 100 s was added to minimise chance of this occurring during a run, to make total wait time of 300 s.

Other than the fluctuations caused by the laser instability, additional fluctuations were seen in periods of rapid acceleration of the drive motors. This occurred on initial acceleration at the start of the pull and at the breaking at the end of the pull. When both upper and lower stages were stationary, heating of the stock is in equilibrium. However, as the upper stage moves faster, this equilibrium status is lost with varying shape and diameter of the fused silica stock, as well as a reduction of incident laser light due to a smaller fibre diameter (figure 7). Therefore, two sets of PID gain values were used for a fabrication process: one for the polishing procedure and another for the pulling procedure.

In figure 8, trials 1–4 show peak pixel intensity data for 4 independent pull processes under the same conditions, and one blue line that stands out indicates the velocity of the upper stage. All 4 trials show a consistent fluctuation pattern at the beginning and at the end with an average percentage error of 26%, while the middle section without fluctuations shows an average percentage error of 1.6%. The starting point of the fluctuation varied slightly for each run, but they all consistently fell in the range where the motor speed varied. Therefore, the PID parameters were adjusted as soon as the motor starts to move, to take the motor speed change into account. Another significant factor to consider is the change in the diameter of the stock. As the pull continues, the diameter of fused silica stock rapidly decreases, from 3 mm to 800 μm and ultimately to 400 μm. In addition, more of the beam misses the stock when the heating region becomes narrower, changing the equilibrium of the heating. Therefore, the new set of

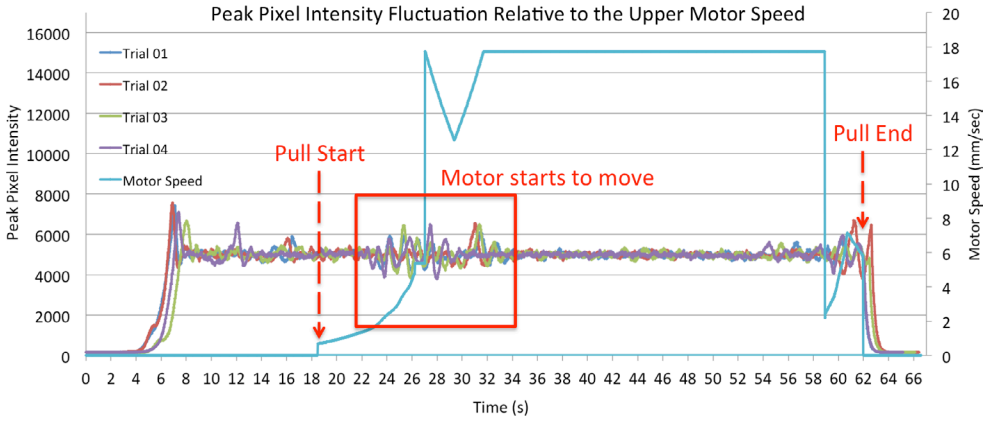

Figure 8. Correlation between the pixel intensity stability and upper motor velocity variation.

PID gains were used when the diameter of the heating region decreased to take the impact of rapid diameter change into account. This adjustment eliminated consistent fluctuation patterns during the pull, showing a similar level of average percentage error as the middle section of the pull (2%). This live PID gain adjustment technique was developed for this fibre pulling system, but it also has potential applications in other engineering areas such as dynamic response in mineral processing [27].

2.4. Polish duration

According to previous research, the polishing conditions including polishing duration could also have an impact on fibre strength [23]. Polishing durations of 2200 s and 3000 s produced stronger fibres on average [23]. Therefore, 900 s, 2200 s, and 3000 s polishes were compared. The polishing duration was controlled by changing the drive voltage of the lower stage. For each condition, 24–30 fibres were produced for strength tests. Detailed description of the polishing process is provided in [23].

3. Results

3.1. Intensity stability comparison

With an optimised recipe for stabilised heating, pulls using this system were compared to the current unstabilised aLIGO pulling technique. Figure 9 shows the comparison between unstabilised and stabilised pulls. The green line shows a typical peak pixel intensity variation during an unstabilised pull, and the red line shows one of the worst unstabilised pulls with more drastic pixel intensity variation. The blue line shows the peak pixel intensity data of a typical stabilised pull. The stabilised pull showed almost constant pixel brightness near the setpoint of 6000. By contrast, for the unstabilised pull, the pixel brightness varied from 3883 to 12 057 for a typical pull and from 1000 to 16 383 for the worst pull, and fluctuated continuously for the full pull. The average peak pixel intensity throughout the pull for the unstabilised pulls was 7429 for a typical pull and 9843 for the worst pull, while that of a typical stabilised pull was 5997. In addition, the standard deviation of unstabilised pulls was 1914 (typical pull) and

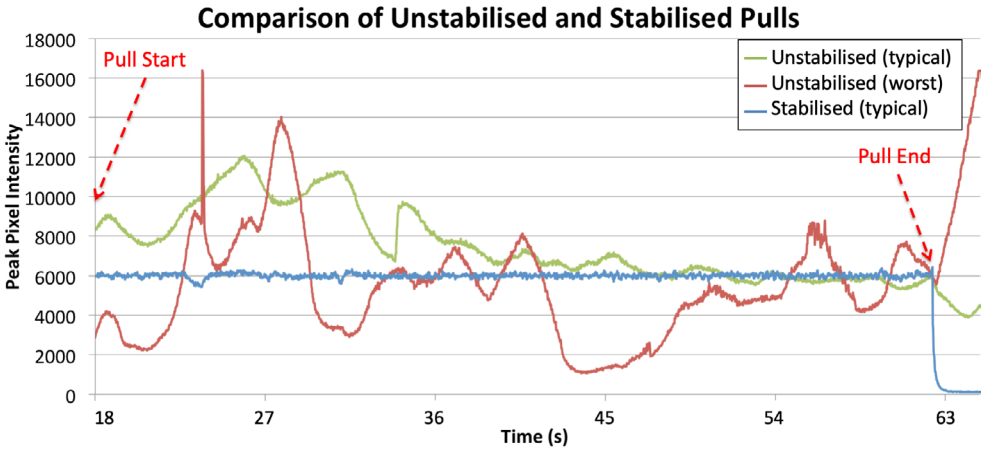

Figure 9. Comparison of peak pixel intensity variation between an unstabilised pull and a stabilised pull.

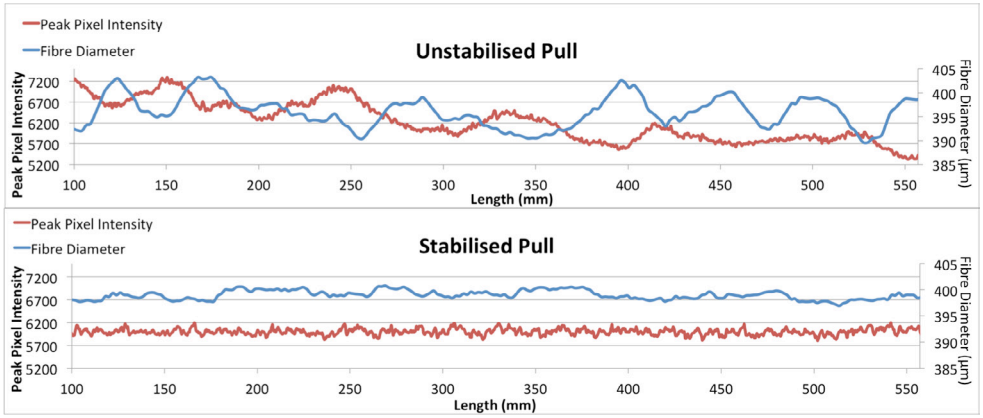

Figure 10. Comparison between the peak pixel intensity and the fibre diameter profile for a typical unstabilised and a typical stabilised pull.

2294 (worst pull), while that of the typical stabilised pull was 84. These results confirm that the intensity stabilisation can keep the heating intensity much more consistent.

This was also confirmed by diameter profile analysis. Compared to 'unstabilised fibres' (fibres produced without the stabilisation system), 'stabilised fibres' (fibres produced with the stabilisation system) not only showed 10.7% decrease in the standard deviation of the diameter (from 5.4 to 4.82), but also showed 19.7% decrease in the spread of average diameter (from 3.46 to 2.8). Since the heating and pulling of fibres is a complex process and the thermal and mechanical properties are very non-linear functions of external parameters such as power, it is likely that values quoted will not directly correlate in magnitude. The range of average diameter over all fibres also decreased from '388 to 404 μm' to '394 to 402 μm'. Figure 10 shows a comparison between the peak pixel intensity and the fibre diameter profile for a typical unstabilised and a typical stabilised pull. This result proves that the stabilisation system allows better control over the fibre's geometry.

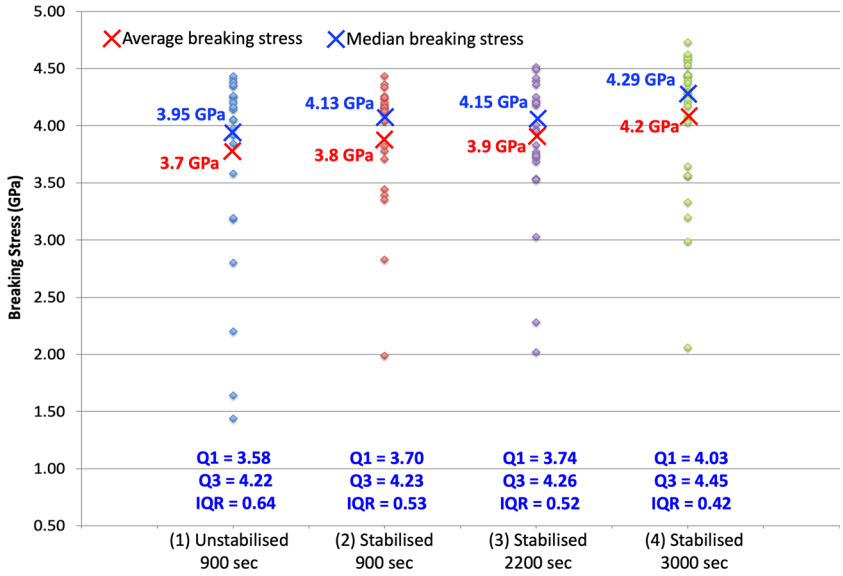

Figure 11. Strength test result comparison between different conditions: (1) current aLIGO condition, without stabilisation, 900 s polish, (2) stabilised, 900 s polish, (3) stabilised, 2200 s polish, (4) stabilised, 3000 s polish. Stabilised fibres showed 34% decrease in interquartile range (IQR) compared to unstabilised fibres.

3.2. Strength tests

After measuring the profile of the fibres, a tensile strength test was performed to check the breaking strength of each fibre.

Each fibre was clamped into the strength test machine, with the upper clamp connected to a load cell and the lower clamp gradually driven down to increase the load on the fibre. When the fibre broke, the maximum load was recorded by the load cell. Since the strength of the silica is highly dependent on the surface cracks, both ends of the stock could not be directly clamped by the toothed faces of the clamps. Instead, a resilient interface layer was introduced with both fibre ends attached to cardboard pieces by Araldite 2-component epoxy adhesive. While curing, the fibres were left in uncontrolled environment, as all previous fibres had been hung in such environment for periods of up to a year with no obvious ill effects.

Figure 11 shows a comparison of strength test results between different conditions: (1) current aLIGO condition, without stabilisation, 900 s polish, (2) stabilised, 900 s polish, (3) stabilised, 2200 s polish, (4) stabilised, 3000 s polish. (1) and (2) show the direct comparison between the unstabilised and the stabilised condition. (3) and (4) were compared to further investigate the effect of different polishing conditions. The data shows that the stabilised pulls have a smaller spread in breaking stress. This is also confirmed by comparing the interquartile range (IQR), with stabilised fibres showing 34% decrease in IQR compared to that of unstabilised fibres. In addition, the stabilisation system increased the minimum breaking stress of the fibres. All stabilised fibres had breaking stresses greater than 2 GPa, which is comfortably above the potential suspension upgrade condition of 1.2 GPa. With a longer polish duration of 3000 s, the average breaking stress of stabilised fibres showed a 9% increase and the median breaking stress showed a 8.6% increase, over the unstabilised fibres. Not only is the maximum breaking stress increased, but also the percentage of fibres which have breaking stress greater

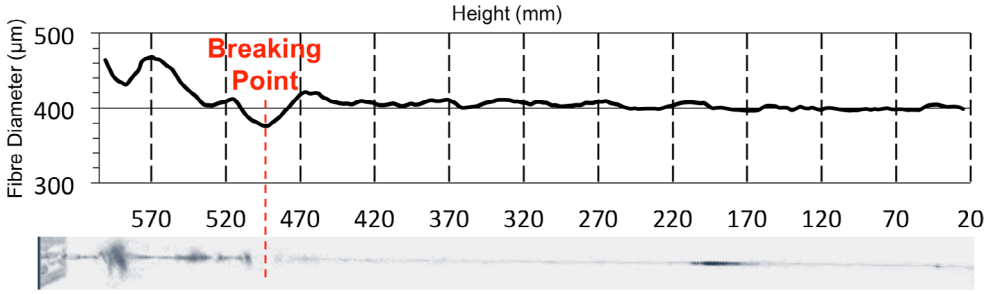

Figure 12. Fibres diameter profile data overlaid on a screenshot of the breaking moment taken by a high speed camera. For clarity, the image colour was inverted. A red line indicates the breaking point of the fibre.

than 4 GPa, which increased from 60% to 80%. This result indicates that heating intensity stabilisation, can improve the reproducibility of fibre fabrication.

3.3. Breaking point analysis

To confirm how the diameter fluctuations due to laser instability can influence the breaking of the fibre, a breaking point analysis was performed. A Phantom V710 high speed camera was set up to monitor when each fibre breaks, at frame rate of 22 000 fps. A ruler was attached on the strength tester to quantify the breaking point in respect to the fibre length. Each video frame was carefully investigated to find the breaking point of the fibre. Figure 12 shows a screenshot of the high speed camera video of the breaking moment. The line above the screenshot photo shows the fibre diameter data, and the red line indicates the initial breaking point. To compare the breaking position to the diameter profile data, the stretch of the material needs to be considered. Since fused silica fibres are relatively soft, they stretch significantly during tensile load application: 20 mm for fibres with breaking stress of 3 GPa and 33 mm for fibres with breaking stress of 4.6 GPa. Therefore, taking account of the stretch of the fibre at the breaking moment, the breaking point and fibre diameter data were adjusted and aligned to compare. The minimum diameter point was checked first, and if that did not match, the fibre profile was investigated further to see if there were any equivalent thin points around that breaking range.

Figure 13 shows the comparison between the diameter profile, laser fluctuation, and the breaking point. The minimum diameter point, which correlates with the breaking point, coincides with this fluctuation point. This tendency was consistently observed in other fibres. Only 7.4% out of 108 fibres did not break at their minimum diameter point but at random points. This result suggests that we can distinguish fibres with potential weak points just by investigating the intensity stability during the pull, before we even test the strength or profile the diameter of the fibres, and that the more stable the pull the less likely there will be variations.

4. aLIGO upgrade option investigation

From both the profile data and strength test results, it has been observed that the statistical strength and dimensional reproducibility of silica fibres can be enhanced by implementing our intensity stabilisation system and varying the pulling and the polishing conditions. The significance of this enhancement is that the A+ upgrade for aLIGO proposes to install thinner fused silica fibres to enhance the sensitivity, and it is essential to improve and confirm the reliability

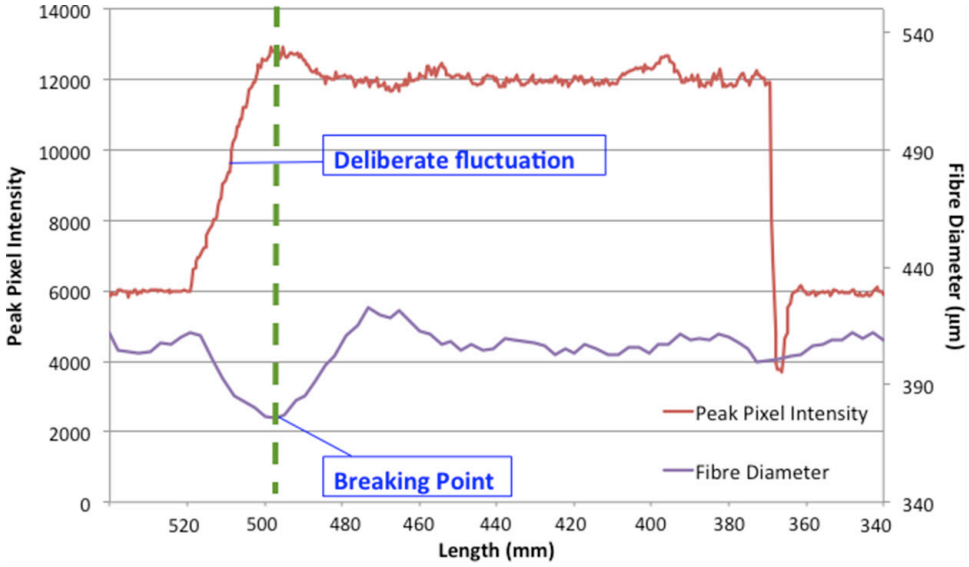

Figure 13. Comparison between peak pixel intensity data of a pull where a deliberate fluctuation was placed in the middle of pulling process and the corresponding fibre diameter profile.

Table 1. Parameters for the current aLIGO suspension and Upgrade #1, #2, #3, #4.

	Test mass (M_4)	Final stage length (L_4)	Total suspension length (L_{Total})	Stress in fibers
aLIGO condition	40 kg	0.6 m	1.6 m	770 MPa
Upgrade #1	40 kg	0.6 m	1.6 m	1.2 GPa
Upgrade #2	40 kg	1.1 m	2.14 m	1.2 GPa
Upgrade #3	80 kg	1.1 m	2.14 m	1.2 GPa
Upgrade #4	160 kg	1.1 m	2.14 m	1.2 GPa

of thinner fibres. Currently, multiple upgrade plans for aLIGO beyond A+ are being studied [28]. Changing the mass, stress, and length of the mirror suspensions are all being considered to reduce noise sources.

Increasing the mass of the test masses, as well as the total suspension mass can improve different noise sources such as suspension thermal noise and radiation pressure noise [28]. For this simulation, the current aLIGO test mass condition of 40 kg, and increased mass of 80 kg and 160 kg were compared. For the static stress in the thin section of the fibre, the current aLIGO condition of 770 MPa was compared to the potential upgrade option of 1.2 GPa. As it was possible to achieve the average breaking stress of 4.2 GPa utilising enhanced fibre fabrication technologies, a stress of 1.2 GPa was chosen to give a reasonable safety factor greater than 3. Having longer fibres for the last stage of the suspension can also improve the suspension thermal noise [17]. Two situations were compared; (1) the current aLIGO length of 0.6 m, (2) 1.1 m which is the maximum length allowed in the current vacuum chamber.

For convenience, Upgrade #1, #2, #3, #4 are defined as following (table 1):

Using a Matlab code, the suspension thermal noise of current aLIGO, and four other upgrade options were investigated. The mechanical dissipation in fibres suspending a mass

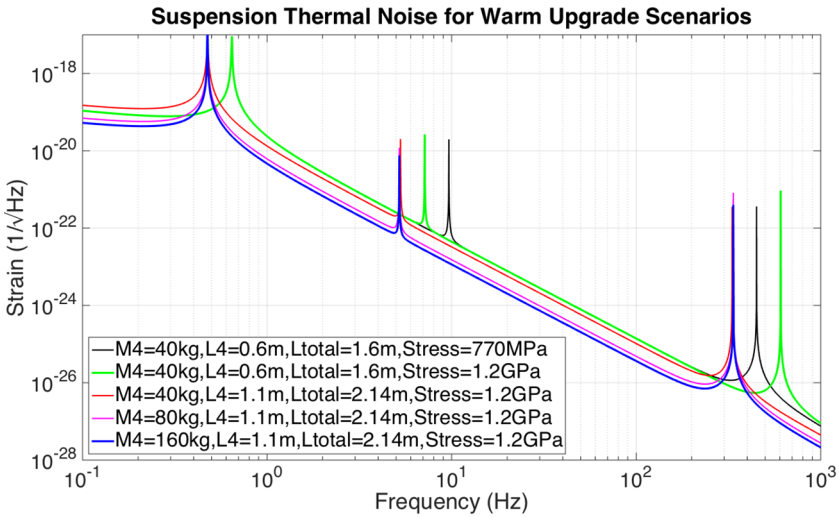

Figure 14. Suspension thermal noise simulation of different upgrade options compared to the current aLIGO condition. This figure does not include other noise sources such as gravity gradient noise, coating Brownian noise and radiation pressure noise.

such as a mirror consists of surface loss, bulk loss, and thermoelastic loss [29]. Surface loss can result from a variety of sources, for example cracks and contamination on the surface of the fibre [23]. From previous studies, it is known that the effect of surface loss on the total loss of fibre has a diameter dependence [23, 30]. Since the fibre has a very high surface to volume ratio, the impact from surface loss is significantly greater than that of bulk loss. Bulk loss is the term given to internal friction occurring in the volume of the material, and is the dissipation due to inherent material microstructure [31]. Thermoelastic loss is the energy loss caused by the internal heat transfer due to the thermal expansion coefficient of the fibre [32, 33]. Temperature fluctuations cause the fibre to be heated or cooled, which results in simultaneous expansion and compression of the fibre, introducing another displacement noise source in the detector. From the definition of thermoelastic loss [10], there is a possibility that it can be totally cancelled out by controlling the stress applied to the fibre. Therefore, fused silica fibres are made with a dumbbell shape, where the bending regions of the fibre have a specific diameter for thermoelastic noise cancellation, and the middle section of the fibre has smaller diameter to optimise resonance frequencies like lowering the vertical mode frequency to below the observation band of the detector [6, 34]. If the thermoelastic loss can be minimised, the surface loss will have the dominant impact on total loss [35].

Figure 14 shows the Matlab modelling results of suspension thermal noise for different conditions. With higher stress and a longer final stage, the vertical bounce mode frequency and the overall thermal noise level were improved. Even the minimal change option, Upgrade #1, showed a factor of 2.5 improvement in suspension thermal noise at 10 Hz, by pushing down the resonance frequency. For other upgrade options, the overall suspension thermal noise was improved due to longer final stage and heavier test mass. For Upgrade #4, the noise at 10 Hz was improved by factor of 5. Not only is the overall thermal noise level lower but also the vertical bounce mode frequency was lowered. For the current aLIGO condition, the vertical bounce mode frequency was 9.8 Hz while Upgrade #1 moved it down to 7 Hz and other options pushed it even further down to 5.2 Hz. Other than bounce mode frequency, the first violin mode frequency went up to 616 Hz for Upgrade #1 and decreased to 350 Hz for other

upgrade options while that of the current aLIGO value is 512 Hz, and the pendulum mode frequency decreased from 0.66 Hz to 0.46 Hz as the length of the final stage increased. This improvement will help further expanding the detection band of aLIGO detectors.

Implementing the fibre fabrication technologies explained above, we can achieve these upgrade options to further improve the aLIGO detection band by lowering the suspension thermal noise especially in the lower frequency range. Even for increased stress of 1.2 GPa, we can still have a safety factor of 3.5 away from average breaking stress. Note that fibres with low breaking stress could be eliminated by pre-tests, hanging the fibres under high stress before implementing it to the real suspensions—a test already part of the standard aLIGO installation procedure. Improved sensitivity in the lower frequency detection band will allow observations of more astronomical sources with higher accuracy in source parameter estimations as signals will spend longer length of time in the observation band.

5. Conclusions

To improve the statistical strength of fused silica suspension fibres for aLIGO monolithic suspensions, heating intensity stabilisation was investigated and various conditions for the polishing and pulling processes were optimised. By comparing the peak pixel intensity data to the profiled fibre geometry data, it was shown that the heating intensity can influence the fibre geometry. With the PID controlled stabilisation system, the heating intensity of the stock was kept constant around the setpoint with an average peak pixel intensity of 5997 and average standard deviation of 38.5. To ultimately check the maximum load of the fibres, tensile strength tests were performed, and the result of 'unstabilised' and 'stabilised' pulls were compared. Stabilised fibres showed a 37.5% smaller standard error of the mean breaking load, compared to unstabilised ones. For stabilised fibres, none of the fibres had breaking stress below 2 GPa. With a longer polishing duration on top of the stabilisation system, the average breaking stress increased by 9% and the median also increased by 8.6%. This result indicates that the application of intensity stabilisation technology can improve the statistical strength of fused silica fibres. Higher stress in the fibre and a longer final stage can improve the sensitivity of an upgraded gravitational wave detector via reduction in thermal noise. Thus, these enhanced technologies will enable us to fabricate thin and robust fibres that can achieve future suspension upgrade requirements, which aim to improve the noise in and around 10 Hz. As the next upgrade plan for aLIGO detectors, the A+ upgrade, plans to utilise thinner fibres, this technique can be directly implemented to provide suitable improved fibres.

Acknowledgment

The authors would like to acknowledge our colleagues in the Institute of Gravitational Research, LIGO Scientific Collaboration, the GEO600 project, and the Scottish Universities Physics Alliance for their interest in this work. The authors would also like to thank Colin Craig and Stephen Craig for their work in manufacturing components for the experiment.The authors would like to thank the Science and Technology Facilities Council (Grant ref: ST/N005422/1) for their financial support. The authors gratefully acknowledge the support of the United States National Science Foundation for the construction and operation of aLIGO and the LIGO laboratories. This paper has LIGO document number LIGO-P1800189.

ORCID iDs

Kyung-Ha Lee https://orcid.org/0000-0003-0470-3718

References

[1] Abbott B *et al* 2016 *Phys. Rev. Lett.* **116** 061102
[2] Abbott B *et al* 2017 *Phys. Rev. Lett.* **119** 161101
[3] Fairhurst S 2009 *New J. Phys.* **11** 123006
[4] Aasi J *et al* 2015 *Class. Quantum Grav.* **32** 074001
[5] Acernese F *et al* 2015 *Class. Quantum Grav.* **32** 024001
[6] Aston S *et al* 2012 *Class. Quantum Grav.* **29** 235004
[7] Harry G *et al* 2010 *Class. Quantum Grav.* **27** 084006
[8] Braginsky V *et al* 1996 *Phys. Lett.* A **2–18** 164–6
[9] Cumming A *et al* 2012 *Class. Quantum Grav.* **29** 035003
[10] Cagnoli G and Willems P 2002 *Phys. Rev.* B **65** 174111
[11] Ageev A *et al* 2004 *Class. Quantum Grav.* **21** 3887–92
[12] Traeger S *et al* 1997 *Phys. Lett.* A **225** 39–44
[13] Taniwaki M *et al* 1998 *Phys. Lett.* A **246** 37–42
[14] GWINC website 2019 (http://git.ligo.org/gwinc)
[15] Gair J *et al* 2011 *Gen. Relativ. Gravit.* **43** 485
[16] Amaro-Seoane P and Santamaria L 2010 *Astrophys. J.* **722** 1197–206
[17] Hammond G 2013 LIGO-G1300660 *Amaldi 10*
[18] Sathyaprakash B *et al* 2012 *Class. Quantum Grav.* **29** 124013
[19] Pankow C *et al* 2018 *Astrophys. J. Lett.* **854** 2
[20] Heptonstall A *et al* 2010 *Class. Quantum Grav.* **27** 035013
[21] Heptonstall A *et al* 2011 *Rev. Sci. Instrum.* **82** 011301
[22] Proctor B and Whitney I 1967 *Math. Phys. Sci.* **297** 534
[23] Heptonstall A *et al* 2014 *Class. Quantum Grav.* **31** 105006
[24] Inc. FLIR Systems 2017 (http://www.flir.com/science/display/?id=46623)
[25] Cumming A *et al* 2011 *Rev. Sci. Instrum.* **82** 044502
[26] Fender R and Hendry M 2000 *Mon. Not. R. Astron. Soc.* **317**
[27] Barker I *et al* 1983 *IFAC Proc.* **16, 15** 1471–6670
[28] Miller J *et al* 2015 *Phys. Rev.* D **91** 062005
[29] Saulson P 1990 *Phys. Rev.* D **42** 2437
[30] Gretarsson A and Harry G 1999 *Rev. Sci. Instrum.* **70** 4081–7
[31] Rowan S *et al* 2012 *Optical Coatings and Thermal Noise in Precision Measurement* (*Substrate Thermal Noise*) ed G Harry *et al* (New York: Cambridge University Press)
[32] Zener C 1937 *Phys. Rev.* **52** 230
[33] Nowick A and Berry B 1972 *Anelastic Relaxation in Crystalline Solids* (London: Academic)
[34] Willems P 2002 *Phys. Lett.* A **300** 162–8
[35] Cumming A 2008 *PhD Thesis* (Glasgow: University of Glasgow)